This is the peer reviewed version of the following article: Zarezadeh-mehrizi, Mohammad Amin, Liaghat, Gholamhossein, Ahmadi, Hamed, Taherzadeh-Fard, Alireza and Khodadadi, Amin (2022) Numerical and experimental investigation of fiber metal laminates with elastomeric layers under low-velocity impact. Polymer Composites, 43(4), pp. 1936-1947, which has been published in final form at https://doi.org/10.1002/pc.26509. This article may be used for non-commercial purposes in accordance with Wiley Terms and Conditions for Use of Self-Archived Versions. This article may not be enhanced, enriched or otherwise transformed into a derivative work, without express permission from Wiley or by statutory rights under applicable legislation. Copyright notices must not be removed, obscured or modified. The article must be linked to Wiley's version of record on Wiley Online Library and any embedding, framing or otherwise making available the article or pages thereof by third parties from platforms, services and websites other than Wiley Online Library must be prohibited.

Remove Watermark Wondershare PDFelement

# Numerical and experimental investigation of fiber metal laminates with elastomeric layers under low velocity impact

Mohammad Amin Zarezadeh-mehrizi [a], Gholamhossein Liaghat [a, b,*], Hamed Ahmadi [a], Alireza Taherzadeh-Fard [a, c], Amin Khodadadi [a]

[a] Mechanical Engineering Department, Tarbiat Modares University, Tehran, Iran
[b] School of Mechanical & Aerospace Engineering, Kingston University, London, England, United Kingdom
[c] Strength of Materials and Structural Engineering Research Group – UPC, Edifici C1, Campus Nord, Barcelona, Spain

## Abstract

This study aims to investigate the effects of elastomers on Fiber Metal Laminates (FMLs) subjected to low-velocity impact loads. A compounded natural rubber layer was added to conventional FMLs containing glass/epoxy composite plies and Al 6061-T6 layers, measuring its effect on the behavior of the structure in low-velocity indentation at energy levels of 25 J and 45 J. It was found that the addition of an elastomeric layer to the back face of the composite layer increased structural toughness, pre-fracture deformation, and specific energy absorption while reducing damage and the maximum load. Moreover, positioning the elastomer at a closer distance to the frontal face reduced maximum load and energy absorption capacity. Then, the standard material characterization of tensile, shear, and compressive were performed via the universal testing machine and the split Hopkinson pressure bar apparatus. A numerical model was developed based on the advanced finite element code of LS-DYNA, and the results were validated by comparison to the experimental data.

**Keywords:** Low velocity Impact, Fiber Metal Laminate (FML), Natural Rubber, Numerical simulation, LS-DYNA

*Corresponding author: Mechanical Engineering Department, Tarbiat Modares University, P.O. Box 14115-111, Tehran, Iran.
E-mail address: ghlia530@modares.ac.ir , Tel. +98-2182883387

Remove Watermark Wondershare PDFelement

## 1. Introduction

In light of design industry developments, the use of composites in a variety of structures has been of great interest in recent decades. The advantages of composites over other materials include low weight, high elasticity, proper ductility, and high flexibility, representing an ideal material for various industries[1-3]. However, composite structures have a variety of drawbacks, including heterogeneity, high moisture absorption, low heat resistance, low abrasion resistance, and low impact loading strength[4-6]. Through a combination of isotropic properties, plastic behavior, high durability and stability, impact resistance, and easy repair of metals with high strength properties, optimal stiffness, high fatigue life of composites, FMLs emerged as an ideal alternative. The main purpose of designing and manufacturing FMLs is to simultaneously exploit the excellent properties of metal and composites[7-9]. In light of higher performance than other corrosion-resistant materials, FMLs have been widely used in the aviation industry. Fabricating the fuselage of the Airbus 380 with a GLARE made it possible to reduce the weight by 794 kg[8]. In recent years, various tests have been performed on FMLs to study their impact loading behavior. Partial plastic deformation under low-velocity impacts is the most common impact damage in FMLs[10, 11]. Since aluminum is a ductile material, impact loads cannot have devastating effects on aluminum components; aluminum can absorb a large amount of impact energy through large deformation both in the elastic and plastic regions. In contrast, most composites are inherently brittle and can only absorb energy in the elastic region. In the absence of plastic deformation, damage to the composites is difficult to characterize until complete failure. As a result, they may abruptly lose the load-bearing capacity[12].

Numerous studies have been conducted to increase the stiffness of structures under impact loads, crack growth resistance (crack bridging), and shear deformation capacity[13-16]. Research has

Wondershare PDFelement

Remove Watermark Wondershare PDFelement

shown that the integration of elastomers with brittle materials (e.g., composites) can enable the composite to withstand more deformation before failure and increase energy absorption in most cases[1, 17-22]. Segrety et al. (2004)[19] experimentally studied the low-velocity impact loading of elastomer-reinforced and non-reinforced PMMA polymers. In the non-elastomeric specimens, many cracks propagated at low displacements, and elastomer reinforcement increased deformability before failure. Mohotti et al. (2014)[1] examined the plastic deformation of aluminum/composite sheets coated with polyurea with a thickness of 6-12 mm at low velocities (5-15 m/s). In addition to experimental tests, a numerical model was developed with the LS-DYNA code. The polyurethane-coated sheet was found to have lower plastic deformation than the non-reinforced sheets. This indicates that polyurea increased energy absorption and energy dissipation. Düring et al. (2015)[6] studied the low-velocity impact loading of the hybrid glass and carbon composite/steel/elastomer structure experimentally. Load and deformation measurements revealed that the elastomeric layer could increase the destruction load threshold.

The addition of elastomers improves the impact properties, such as interlaminar fracture toughness, matrix fracture stiffness, and diminishes strength, stiffness, and temperature-dependent properties (e.g., glass temperature). The main challenge is to bring a trade-off between these properties[13, 14, 18, 19, 23].

To measure pre-failure energy absorption, impact tests can be carried out. Numerous works sought to obtain the impact resistance of various structures as a crucial material property. In order to ensure the safety and reliability of a structure, it is necessary to examine its behavior under the impact loads[24]. In general, the two common low-velocity impact load tests include (1) drop weight and (2) pendulum testing (Charpy, Izod and tension impact). Since different diagrams (such as load-displacement curves) can be extracted from the drop weight test, it is preferable to use pendulum testing to investigate the impact behavior of materials[25].

Remove Watermark Wondershare PDFelement

The present study mainly aims to modify the GLARE multilayer to enhance energy absorption and reduce damage. To handle the drawbacks of composites under impact loading and increase energy absorption, the present work added an elastomer layer to the structure. Also, the optimal position and thickness of the elastomeric layer were studied experimentally and numerically. This would reduce the cost and increase the lifespan of the structure under environmental impacts (e.g., rock collisions and falling objectives.). The methods and materials of fabricating a high-quality specimen are described. Then, the process of different tests according to the current standards is investigated. Experimental tests and equipment are introduced. The three-dimensional numerical model developed in LS-DYNA[26] is described. Then, the results are provided and discussed. Finally, the work is concluded.

Wondershare PDFelement

## 2. Experimental Procedure

### 2.1. Materials

The hybrid structure was composed of three phases: (1) aluminum, (2) composite, and (3) elastomer. The outer layers were 6061-T6 Al obtained from AMAG rolling GmbH with a nominal thickness of 0.5 mm. Natural rubber (SMR 20) was employed as the elastomeric phase, and ingredients such as calcium carbonate and carbon black (purchased from Yazd Rubber Company) were added in order to improve the mechanical properties. The Mooney viscosity of the compounded elastomer was 65 (purchased from the Rubber Research Institute of Malaysia). Natural rubber was utilized in light of its superior properties such as biodegradability, flexibility, tear resistance, and damping capacity[27, 28]. Moreover, stearic acid, ZnO, accelerators, stearic acid, and sulfur (LG Company) were used in the vulcanization bonding process. The elastomer density was found to be 1255 $kg/m^3$. Table 1 reports the ingredient quantities whilst Table 2 represents

Remove Watermark Wondershare PDFelement

the curing characteristics of the compounded elastomer[29] in which $M_{min}$ and $M_{max}$ are the minimum and maximum vulcanization torques, respectively and $t_i$ represents the required time to reach the i% of maximum torque within the Oscillating Disc Rheometer (ODR) test.

**Table 1.** Formulation of the compounded rubber

| Ingredients | Loading (Phr) |
|---|---|
| NR | 100 |
| Carbon black (N330) | 60 |
| Calcium carbonate | 30 |
| Spindle oil | 15 |
| Zink oxide | 5 |
| Sulfur | 2 |
| Volcacit | 0.7 |

Wondershare PDFelement

**Table 2.** Curing characteristics of the compounded rubber

| Quantity | $t_{50}$ (min) | $t_{10}$ (min) | $t_{90}$ (min) | $t_{95}$ (min) | $t_{100}$ (min) | $M_{min}$ N.m | $M_{max}$ N.m |
|---|---|---|---|---|---|---|---|
| Value | 0.28 | 0.72 | 2.90 | 3.40 | 5.30 | 0.83 | 11.5 |

The composite layer included plain-woven glass fibers (200 gr/$m^2$) and ML-506 epoxy resin obtained from Metyx Co. (Turkey) and Mokarrar Company (Iran), respectively. Two adhesives were utilized to achieve the strongest attachment[30, 31]. The two-component Chemosil adhesive (Chemosil 222 and Chemosil 211 as a primer) was used to bond the elastomer to aluminum, while Bylamet-S2 adhesive was exploited to bond aluminum to the composite and elastomer. Bylamet-S2 (BYLA GmbH) is a one-component cyanoacrylate adhesive based on modified ethylene ester. It has excellent performance in binding rubbers, metals, and plastics.

### 2.2. Fabrication

Remove Watermark Wondershare PDFelement

The composite sheets were fabricated using six glass/epoxy layers and hand layup. Then, the sheets were cut into a nominal size of 12×12 mm. To obtain a rough surface for efficient adhesion, a layer of peel ply was pooled off each side of the composite layer. The composite and aluminum surfaces were modified based on the ASTM D2093 and ASTM D2651 standards, respectively. The modified aluminum layer was impregnated with a thin layer of Chemosil 211 adhesive as a primer and then with a thin layer of Chemosil 222 adhesive. Subsequently, the elastomer was added. The specimen was subjected to hot press for 4 min at 160°C and 25 tons (the temperature and vulcanization time were derived from the rheometer test). Bylamet-S2 adhesive was used to bond the modified composite (D2093 standard)/aluminum and composite/elastomer. Fig. 1 shows the configuration of the specimen. The thicknesses of the elastomer, aluminum, and composite layers were 2.62, 0.5, and 1.91 mm, respectively.

Wondershare PDFelement

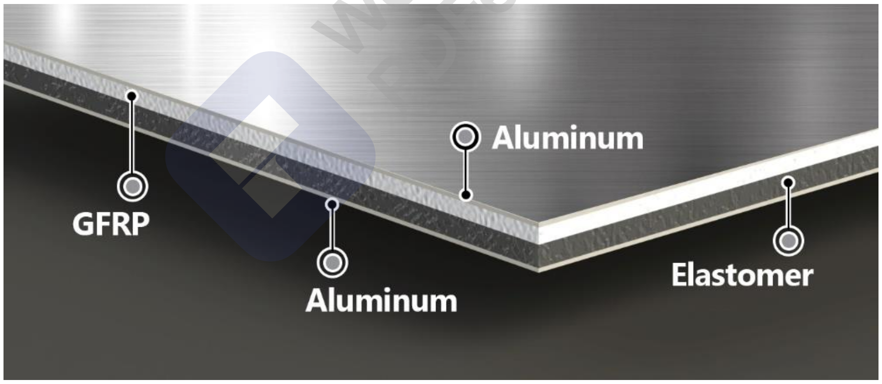


**Fig. 1.** Layer Arrangement of a made sample

### 2.3. Characterization

In order to simulate indentation, it is required to obtain the mechanical properties of all the materials in the structure by characterization tests. Tensile, shear, and compression tests were performed on the glass fiber-reinforced polymer (GFRP) according to ASTM D3039, ASTM

Remove Watermark Wondershare PDFelement

D3518, and ASTM D3410 standards, respectively. The digital image correlation (DIC) method was employed to measure the strain in the longitudinal and transverse directions. Table 3 reports the GFRP properties.

**Table 3.** Mechanical properties of glass/epoxy composite

| **Property** | **Value** |
|---|---|
| Density (kg/m$^3$) | 1479.80 |
| Fiber volume fraction (%) | 40 |
| Young's moduli $E_1$, $E_2$, $E_3$ (GPa) | 19.99 |
| Poisson's ratios, $\upsilon_{12}.\upsilon_{13}.\upsilon_{23}$ | 0.17, 0.414, 0.414 |
| Shear modulus, $G_{12}$, $G_{13}$, $G_{23}$ (GPa) | 1.49 |
| Tensile strengths, $S_1$, $S_2$ (MPa) | 295.45 |
| Compressive strengths, $C_1$, $C_2$ (MPa) | 149.40 |
| Shear strength $S_{12}$, $S_{13}$, $S_{23}$ (MPa) | 91.30 |

Wondershare PDFelement

The Split Hopkinson Pressure Bar (SHPB) was employed to obtain the mechanical properties of the elastomer at different strain rates. To minimize the effects of friction and inertia, the length-diameter ratio of the specimens was set to 0.5, while the specimen length was set to 5 mm to maintain uniform deformation and stress equilibrium in the test. Fig. 2 plots the stress-strain curves of the elastomer obtained in the quasi-static tests at different strain rates.

Remove Watermark Wondershare PDFelement

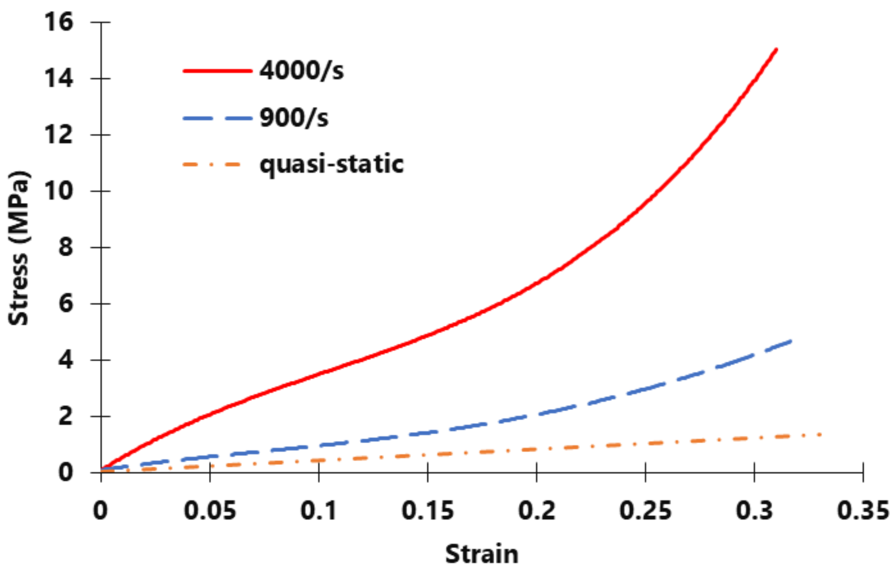


**Fig. 2.** Stress-strain curves for the elastomer at different strain rates

### 2.4. Low-velocity impact test

To conduct the low-velocity impact test, a drop weight along with an accelerometer sensor was exploited. Specimens without an elastomer layer (WE), an elastomer layer positioned on the impacted side (elastomer up or EU), and an elastomer layer positioned on the back of the impacted side (elastomer down or ED) were subjected to steel projectiles, as depicted in Fig. 3. The projectiles had a hemispherical nose shape, a hardness of 53 Rockwell C, and a weight of 6 kg falling from heights of 85 and 50 cm (approximate energy quantities of 45 and 25 J).

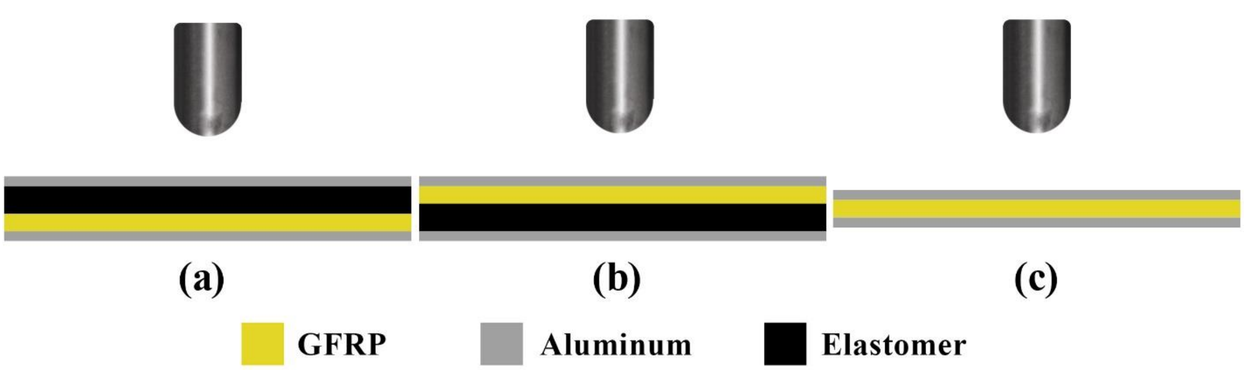

Remove Watermark Wondershare PDFelement

**Fig. 3.** Different configuration of tested specimens, (a) Elastomer Up (EU), (b) Elastomer Down (ED), (c) Without Elastomer (WE)

Drawing on the acceleration sensor outputs, the load-time and load-displacement curves were plotted. Also, energy absorption was calculated. All the specimens were fully clamped in an ST37 steel fixture with a 100-mm square aperture.

## 3. Numerical simulation

### 3.1. Geometric modeling

Wondershare PDFelement

The simulations were performed using commercial finite element code LS-DYNA. To shorten the computational time, a quarter of the geometry was modeled, and symmetric boundary conditions were defined for the symmetric planes of the model. To more accurately describe the stress distribution, eight-node solid elements with reduced integration point formulation were employed. Due to the large stress gradients in the impact area, fine meshes were applied to the impact area, while coarser meshes were used in the adjacency of the edges of the plies. Since boundary conditions strongly influence low-velocity impacts, the clamping frame was modeled to improve accuracy. To implement convergent meshing, the number of elements was gradually increased from 70,000 to 190000. For 140,000 elements (the smallest element size was 0.28 mm), the parameters became independent of the number of elements. Fig. 4 illustrates the finite element model.

Remove Watermark Wondershare PDFelement

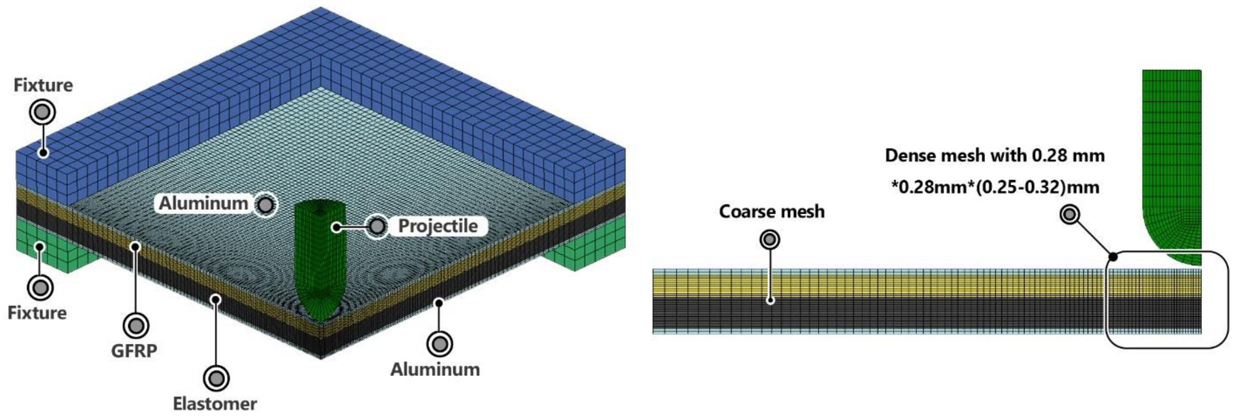


**Fig. 4.** (a) Isometric view and (b) Cross sectional view of the geometry modeling

Wondershare PDFelement

## 3.2. Material models

### 3.2.1. Glass/epoxy composite

To describe the mechanical behavior of laminated composites, LS-DYNA introduces a variety of material models. The present study employed *MAT_COMPOSITE_DAMAGE (MAT_22), which is known as the Chang-Chang material model[32]. MAT_22 is an orthotropic material model with optional brittle failure for composites. This model considers three failure modes as described below:

- Matrix cracking failure criteria is determined from:

$$F_{matrix} = \left(\frac{\sigma_2}{S_2}\right)^2 + \bar{\tau} > 1 \tag{1}$$

Where $\sigma_2$, $S_2$ and $\bar{\tau}$ are transverse stress, transverse tensile strength and fiber matrix shearing term, respectively.

- Compression failure criteria is given as:

$$F_{comp} = \left(\frac{\sigma_2}{2S_{12}}\right)^2 + \left[\left(\frac{C_2}{2S_{12}}\right)^2 - 1\right]\frac{\sigma_2}{S_2} + \bar{\tau} > 1 \tag{2}$$

Remove Watermark Wondershare PDFelement

Where $S_{12}$ and $C_2$ are shear and transverse compressive strengths.

- Fiber breakage mode which is represented as:

$$F_{fiber} = \left(\frac{\sigma_1}{S_1}\right)^2 + \bar{\tau} > 1 \tag{3}$$

In which $\sigma_1$ and $S_1$ are longitudinal stress and strength, respectively.

By satisfying each criteria, the corresponding properties are declined to zero.

In order to prevent instabilities, MAT_ADD_EROSION was incorporated into the model for element deletion after element failure based on a reasonable strain limit criterion.

### 3.2.2. Aluminum

Cowper-Symonds is one of the most common and functional models to simulate aluminum behavior at different strain rates. Simplicity is an advantage of Cowper-Symonds over other formulations. MAT_PLASTIC_KINEMATIC (MAT003) is based on Cowper-Symonds in LS-DYNA[33]. Table 4 reports the parameters of 6061-T6 Al from the literature.

Wondershare PDFelement

**Table 4.** Material constants used for aluminum 6061-T6 in numerical modeling [34]

| $\rho$ (Kg/m$^3$) | $\upsilon$ | $\sigma_Y(MPa)$ | $E_T(MPa)$ | $E(GPa)$ | $\sigma_U(MPa)$ | $Failure\ strain$ (%) |
|---|---|---|---|---|---|---|
| 2700 | 0.33 | 275 | 900 | 68.9 | 332 | 25 |

### 3.2.3. Elastomer

The Mooney-Rivlin material model was used to simulate the hyperelastic behavior of elastomers in LS-DYNA[33]. The strain energy density function was exploited as:

Remove Watermark Wondershare PDFelement

$$W = A(I-3) + B(II-3) \quad (4)$$

in which $2(A+B)$ is the shear modulus of linear elasticity, while I, II, and III are the invariants of the right Cauchy-Green deformation tensor. Also, coefficients A and B are obtained by the curve-fitting of the stress-strain curve in the Hopkinson test. After a series of primary simulations and obtaining the strain rate range, A and B were obtained to be 1.833 and 0.500 MPa, respectively, by least-square curve-fitting.

Similar to composite modeling, MAT_ADD_EROSION was attached to MAT_MOONEY-RIVLIN_RUBBER for element deletion after element failure based on a reasonable strain limit criterion to prevent instabilities.

### 3.3. Delamination modeling and other considerations

Wondershare PDFelement

CONTACT_AUTOMATIC_SURFACE_TO_SURFACE_TIEBREAK with option 6 was applied to the aluminum/elastomer and aluminum/composite interfaces. In this contact, debonding occurs once the interfacial shear and normal stresses satisfy the following non-equality.

$$\left(\frac{|\sigma_n|}{NFLS}\right)^2 + \left(\frac{|\sigma_s|}{SFLS}\right)^2 \geq 1 \quad (5)$$

Where $\sigma_n$ and $\sigma_s$ are current developed normal and shear stresses whilst NFLS and SFLS are interfacial normal and shear strengths, respectively. This could be considered as an effective way in simulating delamination between engaged layers in the contact. According to the Bylamet-S2 adhesive manufacturer's datasheet, the interlaminar normal and shear strength of the aluminum/composite interface were set to 17 and 19 MPa, respectively. Moreover, the interlaminar normal and shear strength of the elastomer/aluminum interface were found to be 130 MPa[35]. Since the elastomeric and composite layers did not separate,

Remove Watermark Wondershare PDFelement

CONTACT_TIED_SURFACE_TO_SURFACE was applied to the elastomer/aluminum interface[36].

CONTACT_AUTOMATIC_SURFACE_TO_SURFACE was applied to the non-adjacent layers, whereas CONTACT_ERODING_SURFACE_TO_SURFACE with a segment-based formulation was applied to the projectile and target[37] considering static and dynamic coefficients of friction of 0.2 and 0.15, respectively[29].

## 4. Results and discussion

The impact test was performed at energy levels of 25 and 45 J. The results of these two energy levels are discussed separately.

Wondershare PDFelement

### 4.1. 25-J impact

At an energy level of 25 J, the projectile jumped back after impacting the specimens. Fig. 5 plots the load-displacement curves of specimens EU, ED, and WE for better comparison. To analyze the results, different criteria, such as the curve slope (dynamic stiffness), maximum load, energy absorption, and deformation at the maximum load are reported in Table 5.

Remove Watermark Wondershare PDFelement

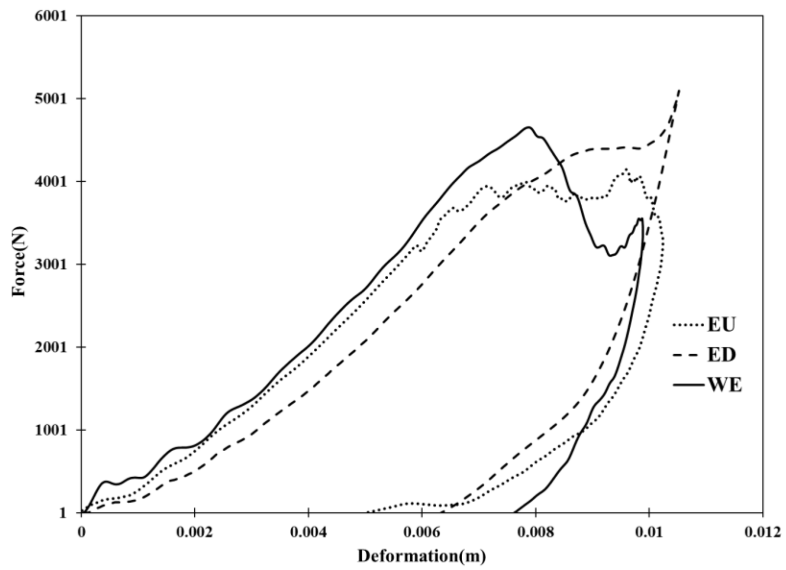


**Fig. 5.** Force-deformation diagram for elastomer-up (EU), elastomer-down (ED) and without elastomeric (WE) samples at low velocity impact with 25 joules of energy

**Table 5.** Drop weight test data from a height of 50 cm (25 J energy)

| Arrangement | Max Force (N) | Energy absorption (J) | Deformation in Max Force (mm) | Diagram slope (N/mm) |
|---|---|---|---|---|
| ED | 5090 | 18.1 | 10.5 | 485 |
| EU | 4145 | 20.91 | 9.64 | 574 |
| WE | 4650 | 22.22 | 7.96 | 584 |

Wondershare PDFelement

According to Table 5, the elastomer layer reduced the maximum load with a larger or lower effect than WE, depending on the elastomer position. In the case of EU, since the stiffness of the elastomer is low and it is positioned after the aluminum layer in front of the projectile, the maximum load was found to be lower than that of specimen WE. For specimens WE and ED, the projectile strikes a high-strength layer (composite); at a very low displacement, the load rises, leading to composite failure. However, as the elastomeric layer in ED supports the composite and prevents its failure at a low strain, the load exceeds that of WE. It was observed that elastomer

Remove Watermark Wondershare PDFelement

increased deformation at the maximum load for both specimens ED and EU, eliminating the brittleness of the entire structure.

According to Table 5, the addition of the elastomer reduced energy absorption and ultimate deformation. This energy absorption reduction indicates a decrease in damage since the elastomer has high tensile strength and absorbs projectile energy by elastic deformation, being stretched as a spring. Then, elastic energy is re-transported to the projectile, with a small quantity of energy remaining in the specimen in the form of plastic deformation. A comparison of ED and EU indicates that the ED specimens had the lowest energy absorption and highest performance (i.e., minimum damage). This is explained by the fact that the elastomer of ED has a large space for stretching and deformation behind the composite layer; while EU has limited space for stretching and elastic deformation since a composite layer of high rigidity and strength is positioned behind the elastomer layer. According to Table 5, the elastomer reduced stiffness and increased the spring function. This effect was greater in ED in light of a larger stretching space of the elastomer layer.

Wondershare PDFelement

**4.2. 45-J impact**

At an energy level of 45 J, the projectile completely penetrates the specimens. The load-displacement curves of EU, ED, and WE are shown in Fig. 6 for better comparison. Table 6 provides the results.

Remove Watermark
Wondershare PDFelement

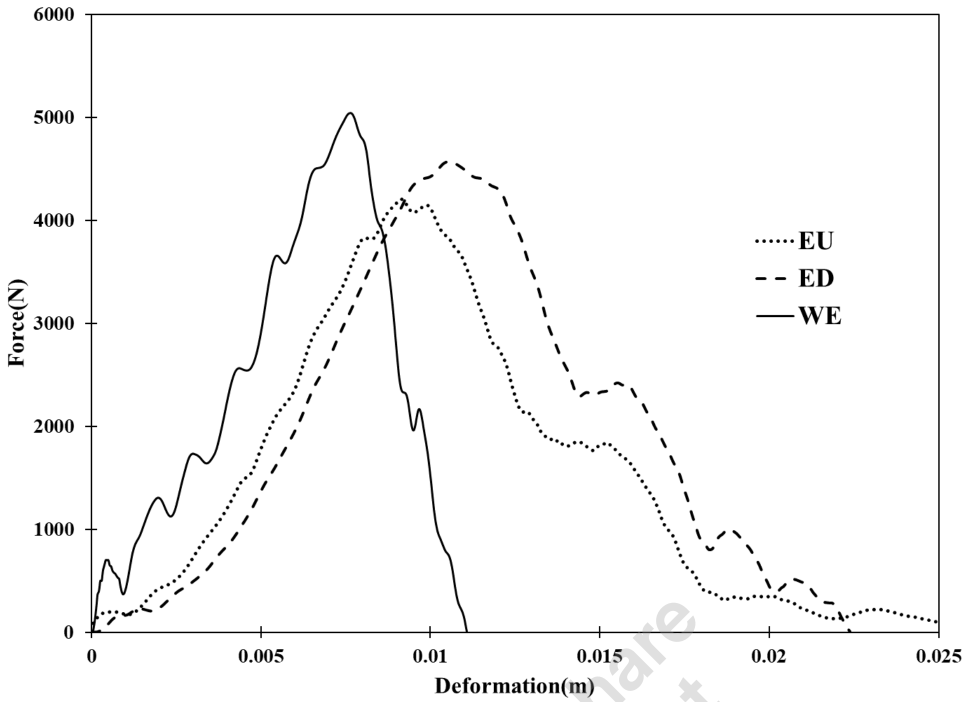


**Fig. 6.** Force-deformation diagram for elastomer-up (EU), elastomer-down (ED) and without elastomeric (WE) samples at low velocity impact with 45 joules of energy

Wondershare PDFelement

**Table 6.** Drop weight test data from a height of 85 cm (45 J energy)

| Arrangement | Max Force (N) | Energy absorption (J) | SEA (J/g) | Deformation in Max Force (mm) | Diagram slope (N/mm) |
|---|---|---|---|---|---|
| ED | 4570 | 44.19 | 0.34 | 10.6 | 432 |
| EU | 4201 | 39.16 | 0.301 | 9.34 | 450 |
| WE | 5038 | 26.81 | 0.333 | 7.64 | 659 |

As can be seen in Table 6, the addition of an elastomer layer to FMLs could reduce the maximum load. To utilize the structure for protective purposes, it is necessary to apply a small load to the target. As a result, the person or equipment suffers from a lower load when subjected

Remove Watermark Wondershare PDFelement

to an impact, diminishing the degree of damage. For a structure serving as a protective layer, an elastomeric layer can reduce damage to the main components. Likewise, the maximum load reduction was found to be greater in EU than in ED. To explain the reduction in the maximum load after the addition of elastomers, it can be said that the composite and aluminum layers had relatively high stiffness, while the stiffness of the elastomers is much lower. The addition of an elastomer layer reduces the stiffness of the structure (the load-displacement slope) and, consequently, the structure reaches the failure strain at a lower load.

According to Table 6, the elastomer increased energy absorption. The increase in energy absorption was greater in ED as it allowed the elastomer to stretch more - EU had lower elastomer deformation due to the composite layer of high rigidity behind the elastomer layer. Also, as a protective layer for the composite, the elastomer increased the deformation of the composite layer and energy absorption. Due to the delayed maximum load in the elastomeric specimens, especially in ED, and the high damping of elastomers, it can be concluded that a larger area of the structure was involved in the impact, leading to a change in local loading into global. As a result, the structure could absorb greater energy under the projectile impact.

Wondershare PDFelement

For structures with a weight limit, it is necessary to consider specific energy absorption (SEA). The SEA of EU was found to be 11.7% lower than that of WE. The SEA of ED showed no decrease compared to WE. Therefore, the elastomer layer not only improved material properties but also slightly decreased the SEA of EU but did not change the SEA of ED.

Reduced stiffness (i.e., the slope of the load-displacement curve) is another advantage of elastomer reinforcement. This increases deformation at the maximum load and reduces the maximum load in elastomeric specimens compared to the non-elastomeric ones. Lower stiffness suggests that the load reaches the maximum level in a longer time, and that the indenter

Remove Watermark Wondershare PDFelement

acceleration reduces at a slower rate. In protective shield applications, therefore, a lower impact load is applied to the shielded subject, reducing possible impact damage.

### 4.3. Comparison of experimental and numerical results

The experimental and numerical results are compared to investigate the performance of the developed model. Fig. 7 compares the numerical and experimental load-displacement curves at 25 and 45 J. As can be seen, the experimental and numerical results are in good agreement, suggesting high performance for the numerical model.

Table 7 reports the important parameters in the study of impact loads (e.g., maximum load, energy absorption, deformation at the maximum load, and the slope of the curve) and provides the differences between the experimental and numerical values. The maximum difference between numerical and experimental results was found to be 10%, indicating that the numerical model had satisfactory performance.

Wondershare PDFelement

Remove Watermark
Wondershare
PDFelement

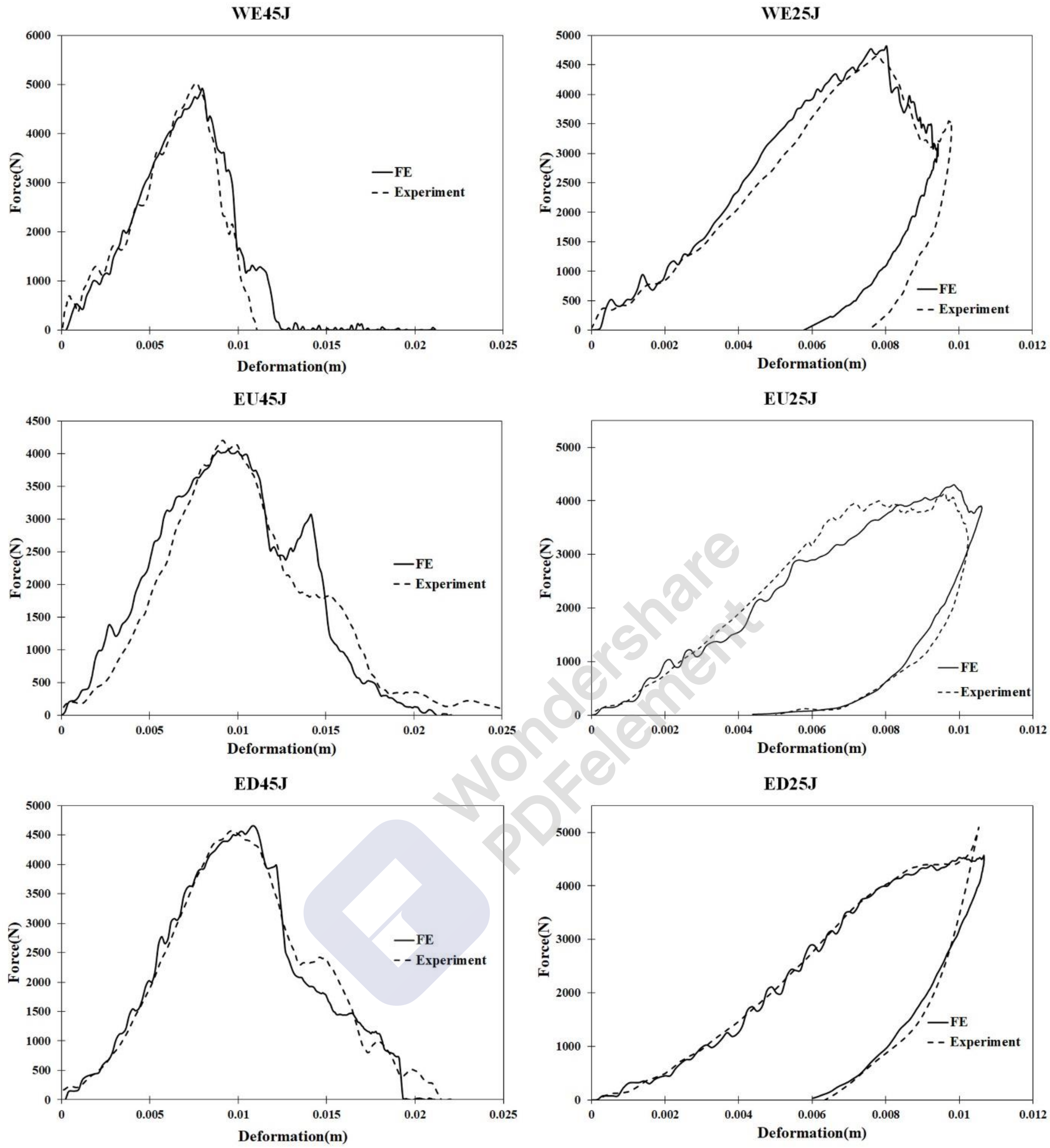


**Fig. 7.** Comparison of force-deformation diagrams from experimental test and numerical simulation

Wondershare
PDFelement

Remove Watermark Wondershare PDFelement

**Table 7.** Comparison of experimental test and numerical simulation results at 25J impact

| | WE | | | ED | | | EU | | |
|---|---|---|---|---|---|---|---|---|---|
| | EXP | FE | Error (%) | EXP | FE | Error (%) | EXP | FE | Error (%) |
| Pick load (N) | 4650 | 4809 | 3.3 | 5090 | 4574 | 10.1 | 4145 | 4303 | 3.7 |
| Absorbed energy (J) | 22.22 | 21.21 | 4.5 | 18.1 | 17.67 | 2.4 | 20.91 | 19.34 | 7.5 |
| Deformation in pick force (mm) | 7.96 | 8.13 | 2.1 | 10.5 | 10.7 | 1.9 | 9.64 | 9.86 | 2.2 |
| Diagram slope (N/mm) | 584 | 591 | 1.2 | 485 | 454 | 6.4 | 574 | 531 | 7.5 |

Table 8 compares four important parameters (maximum load, energy absorption, Deformation in maximum load, Slope of the linear part of the diagram) in the experimental and numerical results at an energy level of 45 J. Also, the numerical and experimental load-displacement curves are plotted in Fig. 7. The numerical results are acceptable as the model was able to predict load-displacement behavior, and the numerical parameters showed a maximum error of 8.5%.

Wondershare PDFelement

**Table 8.** Comparison of experimental test and numerical simulation results at 45J impact

| | WE | | | ED | | | EU | | |
|---|---|---|---|---|---|---|---|---|---|
| | EXP | FE | Error (%) | EXP | FE | Error (%) | EXP | FE | Error (%) |
| Pick load (N) | 5038 | 4922 | 2.3 | 4570 | 4650 | 1.7 | 4201 | 4060 | 3.4 |
| Absorbed energy (J) | 26.81 | 29.3 | 8.5 | 44.19 | 42.86 | 3 | 39.16 | 40.46 | 3.2 |
| Deformation in pick force (mm) | 7.64 | 7.98 | 4.2 | 10.6 | 10.9 | 2.7 | 9.34 | 9.46 | 1.3 |
| Diagram slope (N/mm) | 659 | 617 | 6.3 | 432 | 427 | 1.2 | 450 | 429 | 4.7 |

Remove Watermark Wondershare PDFelement

### 4.4. Failure mechanisms and damage assessment

The specimens were cut using a water jet, determining the failure mechanisms of the section. Fig. 8 depicts the cut sections with the failure mechanisms.

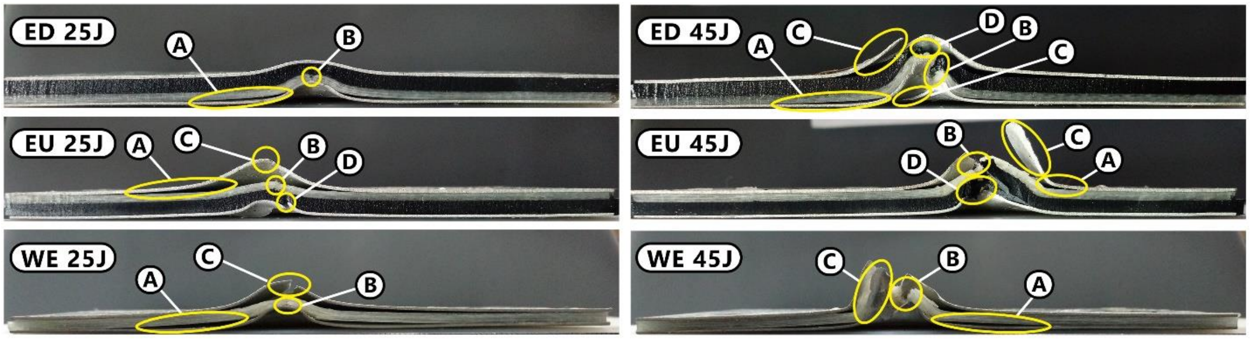


**Fig. 8.** Failure mechanisms and damage assessment

Wondershare PDFelement

Where A represents aluminum/composite delamination, which is mainly due to the impact wave propagation. Indeed, once the indenter touches the surface of the laminate, some compressive waves are spread out in the transverse direction. In the interfaces, a portion of these waves are reflected as the tensile waves, which, in turn, can cause some delamination as depicted in Fig. 8. On the other hand, B denotes fiber breakage, which originates from the tensile stresses as the result of the through-the-thickness movement of the indenter. C represents aluminum petaling, which is the result of the bending moments created by the forward motion of the indenter. D stands for rupture in the elastomeric layer due to tensile stresses and could be referred to as elastomer piercing. Due to the high capacity of rubber in elastic strain recovery, the crater created in the elastomer phase is smaller than the ones in other layers engaged.

As the impact energy increased, more failure mechanisms were activated to absorb energy. At an impact energy level of 25 J, the minimum failure mechanisms were activated; ED showed the lowest ultimate deformation (minimum damage). At a level of 45 J, on the other hand, ED had the

Remove Watermark Wondershare PDFelement

highest energy absorption and the lowest ultimate deformation. As a result, from a damage minimization perspective, ED outperformed the other specimens at both energy levels.


**Fig. 9.** Comparison of samples cross-section from experimental test and numerical simulation

Wondershare PDFelement

Fig. 9 compares the post-impact cross-sections of the specimens in the experimental and numerical models. The proposed numerical model, in addition to the load-displacement curve and impact parameters, was able to predict the failure mechanisms accurately (good agreement with the experimental data). This demonstrates the high performance of the numerical model.

## 5. Conclusion

The present study evaluated the effect of a natural rubber layer added to GLARE on the low-velocity impact response. In addition to the effects of the elastomer on the structure, the optimal position of the elastomeric layer was determined. Subsequently, a numerical model was developed and validated with the LS-DYNA code.

Remove Watermark Wondershare PDFelement

At an energy level of 45 J, ED was found to have the highest energy absorption, highest deformation at the maximum load, highest SEA, longest time to reach the maximum load, lowest stiffness (i.e., load-displacement slope), and smallest ultimate deformation. The advantage of EU over the other specimens was that they had the lowest maximum load.

At an energy level of 25 J, on the other hand, ED showed the lowest energy absorption, penetration depth, stiffness, and damage and the highest deformation in failure and failure time. The only downside of ED was that its maximum contact load was higher than those of the other structures. In contrast, the maximum load of EU was smaller than that of ED and higher than WE. To minimize the maximum load, WT showed the highest performance.

ED showed the highest performance at both 25 and 45 J since it had the highest ability to absorb energy in full penetration and minimize impact damage by enduring larger deformation than the other specimens at 25 J. Also, the maximum load of ED was lower than that of WE at 45 J. To increase energy absorption and reduce damage, ED represents the most effective configuration. To minimize the maximum load (regardless of energy absorption and damage degree), EU is recommended.

**Acknowledgements**

The authors are grateful to Tarbiat Modares University (TMU) for its financial support.

**Declaration of competing interest**

The authors declare that they have no known competing financial interests or personal relationships that could have appeared to influence the work reported in this paper.

**Funding**

Remove Watermark Wondershare PDFelement

This work was supported by Tarbiat Modares University.

## References

.۱ Mohotti D, Ngo T, Raman SN, et al. Plastic deformation of polyurea coated composite aluminium plates subjected to low velocity impact. *Materials & Design (1980-2015)* 2014; 56: 696-713.
.۲ Mohotti D, Ngo T, Mendis P, et al. Polyurea coated composite aluminium plates subjected to high velocity projectile impact. *Materials & Design (1980-2015)* 2013; 52: 1-16. DOI: 10.1016/j.matdes.2013.05.060.
.۳ Sadeghi M, Nienheysen P, Arslan S, et al. Damage detection by double-sided ultrasonic assessment in low-velocity impacted CFRP plates. *Composite Structures* 2019; 208: 646-655.
.۴ Patil NA, Mulik SS, Wangikar KS, et al. Characterization of Glass Laminate Aluminium Reinforced Epoxy-A Review. *Procedia Manufacturing* 2018; 20: 554-562.
.۵ Yang N and Nayeb-Hashemi H. The effect of solid particle erosion on the mechanical properties and fatigue life of fiber-reinforced composites. In: *ASME International Mechanical Engineering Congress and Exposition* 2006, pp.293-299.
.۶ Düring D, Weiß L, Stefaniak D, et al. Low-velocity impact response of composite laminates with steel and elastomer protective layer. *Composite Structures* 2015; 134: 18-26.
.۷ Sinmazçelik T, Avcu E, Bora MÖ, et al. A review: Fibre metal laminates, background, bonding types and applied test methods. *Materials & Design* 2011; 32: 3671-3685.
.۸ Wu G and Yang J-M. The mechanical behavior of GLARE laminates for aircraft structures. *Jom* 2005; 57: 72-79.
.۹ Remmers JJC. Discontinuities in materials and structures: a unifying computational approach. 2006.
.۱۰ Zhu S and Chai GB. Low-velocity impact response of fibre–metal laminates–Experimental and finite element analysis. *Composites Science and Technology* 2012; 72: 1793-1802.
.۱۱ Payeganeh GH, Ghasemi FA and Malekzadeh K. Dynamic response of fiber–metal laminates (FMLs) subjected to low-velocity impact. *Thin-Walled Structures* 2010; 48: 62-70.
.۱۲ Chai GB and Manikandan P. Low velocity impact response of fibre-metal laminates–A review. *Composite Structures* 2014; 107: 363-381.
.۱۳ Nash N, Young T, McGrail P, et al. Inclusion of a thermoplastic phase to improve impact and post-impact performances of carbon fibre reinforced thermosetting composites—A review. *Materials & Design* 2015; 85: 582-597.
.۱۴ Kaynak C, Sipahi-Saglam E and Akovali G. A fractographic study on toughening of epoxy resin using ground tyre rubber. *Polymer* 2001; 42: 4393-4399.
.۱۵ Khodadadi A, Liaghat G, Bahramian AR, et al. High velocity impact behavior of Kevlar/rubber and Kevlar/epoxy composites: A comparative study. *Composite Structures* 2019; 216:.۱۵۹-۱۶۷
.۱۶ Khodadadi A, Liaghat G, Taherzadeh-Fard A, et al. Impact characteristics of soft composites using shear thickening fluid and natural rubber–A review of current status. *Composite Structures* 2021; 271: 114092. DOI: https://doi.org/10.1016/j.compstruct.2021.114092.
.۱۷ Bao S and Tjong S. Impact essential work of fracture of polypropylene/montmorillonite nanocomposites toughened with SEBS-g-MA elastomer. *Composites Part A: Applied Science and Manufacturing* 2007; 38: 378-387.

Wondershare PDFelement

Remove Watermark Wondershare PDFelement

.۱۸ Krollmann J, Schreyer T, Veidt M, et al. Impact and post-impact properties of hybrid-matrix laminates based on carbon fiber-reinforced epoxy and elastomer subjected to low-velocity impacts. *Composite Structures* 2019; 208: 535-545.
.۱۹ Segreti M, Rusinek A and Klepaczko J .Experimental study on puncture of PMMA at low and high velocities, effect on the failure mode. *Polymer testing* 2004; 23: 703-718.
.۲۰ Stelldinger E, Kühhorn A and Kober M. Experimental evaluation of the low-velocity impact damage resistance of CFRP tubes with integrated rubber layer. *Composite Structures* 2016; 139: 30-35.
.۲۱ Stelldinger E, Kühhorn A and Kober M. Failure Analysis of CFRP Tubes with Integrated Rubber Layers Subjected to Transverse Low-Velocity Impact Loading.
.۲۲ Roland C, Fragiadakis D and Gamache R. Elastomer–steel laminate armor. *Composite structures* 2010; 92: 1059-1064.
.۲۳ Stoll MM, Sessner V, Kramar M, et al. The effect of an elastomer interlayer thickness variation on the mechanical properties of Fiber-Metal-Laminates. *Composite Structures* 2019; 219: 90-96.
.۲۴ Velasco J, Martinez A, Arencon D, et al. Application of instrumented falling dart impact to the mechanical characterization of thermoplastic foams. *Journal of materials science* 1999; 34: 431-438.
.۲۵ Söver A, Frormann L and Kipscholl R. High impact-testing machine for elastomers investigation under impact loads. *Polymer testing* 2009; 28: 871-874.
.۲۶ Hallquist JO and Manual L-DT. Livermore software technology corporation. *Livermore, Ca* 1998.
.۲۷ Zaman HU, Khan MA and Khan RA. Comparative experimental studies of phosphate glass fiber/polypropylene and phosphate glass fiber/natural rubber composites. *Journal of Elastomers & Plastics* 2012; 44: 499-514.
.۲۸ Yang H, Yao X, Zheng Z, et al. Highly sensitive and stretchable graphene-silicone rubber composites for strain sensing. *Composites Science and Technology* 2018; 167: 371-378.
.۲۹ Asemani SS, Liaghat G, Ahmadi H, et al. The experimental and numerical analysis of the ballistic performance of elastomer matrix Kevlar composites. *Polymer Testing* 2021; 102: 107311. DOI: https://doi.org/10.1016/j.polymertesting.2021.107311.
.۳۰ Zarezadeh-Mehrizi MA T-FA, liaghat G, Ahmadi H, Khodadadi A. . Experimental study on the plies adhesion of a novel hybrid laminate composed of aluminum, glass-epoxy composite and natural rubber layers under low velocity impact. *In: Proceedings of The 6th International Conference on Composites: Characterization, Fabrication and Application Tehran, Iran, Conference, Conference* 2018.
.۳۱ Taherzadeh-Fard A Z-MM, Liaghat G, Ahmadi H, Khodadadi A. Investigation on the debonding between different layers in a hybrid aluminum/glass-epoxy/rubber laminate under high velocity impact. *In: Proceedings of The 6th International Conference on Composites: Characterization, Fabrication and Application Tehran, Iran, Conference, Conference* 2018.
.۳۲ Chang F-K and Chang K-Y. A progressive damage model for laminated composites containing stress concentrations. *Journal of composite materials* 1987; 21: 834-855.
.۳۳ Hallquist JO. LS-DYNA keyword user's manual. *Livermore Software Technology Corporation* 2007; 970: 299-800.
.۳۴ Abotula S and Chalivendra V. An experimental and numerical investigation of the static and dynamic constitutive behaviour of aluminium alloys. *The Journal of Strain Analysis for Engineering Design* 2010; 45: 555-565.

Remove Watermark Wondershare PDFelement

.۳۵ Taherzadeh-Fard A, Liaghat G, Ahmadi H, et al. Experimental and numerical investigation of the impact response of elastomer layered fiber metal laminates (EFMLs). *Composite Structures* 2020: 112264.
.۳۶ Mohotti D, Ngo T, Raman SN, et al. Analytical and numerical investigation of polyurea layered aluminium plates subjected to high velocity projectile impact. *Materials & Design* 2015; 82: 1-17.
.۳۷ Sevkat E, Liaw B, Delale F, et al. Drop-weight impact of plain-woven hybrid glass–graphite/toughened epoxy composites. *Composites Part A: Applied Science and Manufacturing* 2009; 40: 1090-1110.

Wondershare PDFelement